REVIEW

Check for updates

Optimization mechanism and applications of ultrafast laser machining towards highly designable 3D micro/nano structuring

Xiaomeng Yang,†[a] Ruiqi Song,†[a] Liang He, [iD][ab] Leixin Wu, [iD][a] Xin He,[a] Xiaoyu Liu,*[a] Hui Tang, [iD][c] Xiaolong Lu,[a] Zeyu Ma[a] and Peng Tian [iD]*[a]

Three-dimensional (3D) micro/nano structures are significant in many applications because of their novel multi-functions and potential in high integration. As is known, the traditional methods for the processing of 3D micro/nano structures exhibit disadvantages in mass production and machining precision. Alternatively, ultrafast laser machining, as a rapid and high-power-density processing method, exhibits advantages in 3D micro/nano structuring due to its characteristics of extremely high peak power and ultra-short pulse. With the development of ultrafast laser processing for fine and complex structures, it is attracting significant interest and showing great potential in the manufacture of 3D micro/nano structures. In this review, we introduce the optimization mechanism of ultrafast laser machining in detail, such as the optimization of the repetition rate and pulse energy of the laser. Furthermore, the specific applications of 3D micro/nano structures by laser processing in the optical, electrochemical and biomedical fields are elaborated, and a valuable summary and perspective of 3D micro/nano manufacturing in these fields are provided.

1 Introduction

The emergence of lasers has accelerated the transformation of traditional manufacturing, providing a new means for modern industrial processing and expanding the strategies for processing modern precision devices.

In various microfabrication technologies, laser processing, as an important type of processing method, is divided into long-pulse laser (nanosecond (10^{-9} s) and longer pulse width than nanosecond) and ultrafast laser (pulse width is shorter than a nanosecond, namely picosecond (10^{-12} s), femtosecond (10^{-15} s) and attosecond (10^{-18} s)).[1] Compared with ultrafast laser processing, the heat-affected zone (HAZ) of long-pulse laser processing has a larger scale. Ultrafast laser processing has a smaller HAZ due to its higher peak power and shorter pulse width. Alternatively, in comparison with other non-contact processing, such as focused ion beam (FIB) and electron beam lithography (EBL), ultrafast laser is more economical and its procession speed is higher and thus is more promising for the fabrication of uniform micro/nano structures at a large

scale.[2] To the best of our knowledge, EBL is always applied to obtain ultrafine nanostructures without a mask (*e.g.*, Cr photomask); however, large-area fabrication during a reasonable period is difficult to be achieved by this type of lithography.[3] Ultrafast laser can flexibly produce a variety of patterns in one step, whereas FIB has limitations in the fabrication of periodic surface structures.[4] Additionally, there is no development and rinsing in ultrafast laser processing; therefore, it has the advantages of few steps, no mask, fast processing and environmental friendliness.[5–7] These merits lead to many applications in a variety of aspects, such as the use of ultrafast laser-induced microexplosion to create and recover high-density polymorphs,[8] ultrafast laser pulse for building photonic lattices,[9] and direct nanowriting in air.[10] Also, these characteristics enable ultrafast laser to achieve ultrahigh precision in the processing of three-dimensional (3D) micro/nano structures. Therefore, ultrafast laser processing, as the forefront of laser processing technology, has attracted wide attention. Previous reviews focused on the principles of processing technologies, such as additive processing, subtractive processing, hybrid processing and other processing.[11–13] Also, the different applications of ultrafast laser processing from a processing point of view were introduced.[14–19] Alternatively, considering various structures, this review focuses on sorting the different 3D micro/nano structures processed by ultrafast laser and the micro/nano devices composed of these structures, as shown in Fig. 1.

[a]*School of Mechanical Engineering, Sichuan University, Chengdu 610065, China. E-mail: liuxiaoyu@scu.edu.cn; tianpeng@scu.edu.cn*

[b]*Med+X Center for Manufacturing, West China Hospital, Sichuan University, Chengdu 610041, China*

[c]*School of Materials and Energy, University of Electronic Science and Technology of China, Chengdu 611731, China*
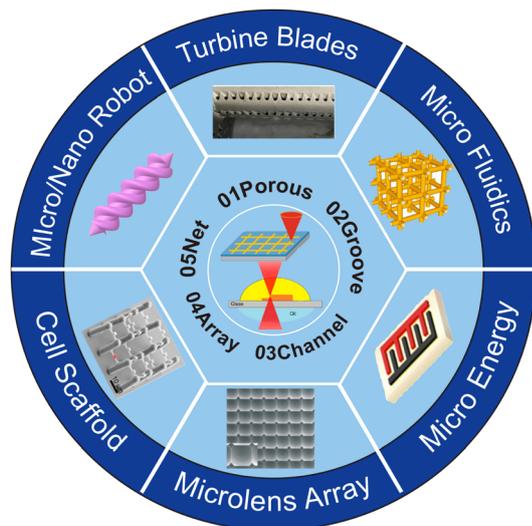
† X. Yang and R. Song contributed equally to this work.

Fig. 1 Schematic diagram of 3D micro/nano structures fabricated by ultrafast laser machining and their applications.[20–26] Reproduced with permission from ref. 20. Copyright 2015, National Academy of Sciences. Reproduced with permission from ref. 21. Copyright 2018, Wiley. Reproduced with permission from ref. 22. Copyright 2021, American Association for the Advancement of Science. Reproduced with permission from ref. 23. Copyright 2018, Elsevier. Reproduced with permission from ref. 24. Copyright 2019, the American Chemical Society. Reproduced with permission from ref. 25. Copyright 2022, Springer Nature. Reproduced with permission from ref. 26. Copyright 2020, Elsevier.

2 Methods and optimization of ultrafast laser

2.1 Principle of laser processing

Ultrafast laser, especially femtosecond laser, has ultra-short pulses of tens to hundreds of femtoseconds, and its energy absorption time is much shorter than the time required by thermal relaxation and other dynamic processes, and thus it can effectively minish the HAZ. The ultrafast laser has a very high instantaneous power, and due to this feature, it can not only process materials with high hardness, but also realize high quality and high precision in 3D processing. Furthermore, the ultrafast laser is capable of fabricating structures with ultra-high machining resolution and extremely small size. Therefore, it has been extensively applied, and the following description elaborates the two most common processing methods.

2.1.1 Ultrafast laser ablation. Femtosecond laser etching (FLE) usually involves the use of a Ti:sapphire laser. The beam emitted by this type of laser is expanded by a beam expander, and afterward focused on the surface of the object through an objective lens. To achieve 3D structures, the modification areas are formed layer-by-layer, which rely on the movement of the XYZ stage. To obtain a more sophisticated 3D structure, this fabrication method usually utilizes femtosecond laser etching in combination with other methods. According to auxiliary operations, there are two types of ultrafast laser etching, *i.e.*, dry etching and wet etching.[27] Wet etching involves exposing the laser to a corrosive chemical solution and it can be employed for

quartz, silicon, glass, *etc.*[28–31] Marcinkevicius and co-workers made pioneering contributions in the wet etching of laser-modified regions.[31] They used femtosecond laser and subsequent etching to fabricate 3D microchannels as small as 10 μm in diameter, with interconnections at arbitrary angles and high aspect ratios (10 μm diameter channels in 100 μm thick silicone plates).[31] Their study indicated that for quartz-based materials, the processing under different etching solutions (hydrofluoric acid (HF) and potassium hydroxide (KOH)) resulted in very different morphologies. Moreover, compared with air ablation, the ablation features in liquid are reduced by 1/3 to 1/2, with higher structural quality and higher resolution.[32] The removal effect in HF is more significant than that in KOH solution due to the fact that the reaction product (SiF_4) is more solvable compared with K_2SiO_3.[32] KOH solution is mainly used for etching silicon-based materials, such as silicon nitride.

Dry etching is often utilized to realize two types of functions. One is to modify various materials by ultrafast laser, and the other is to remove the laser-irradiated area by dry etching.[33–35] Recently, some researchers applied femtosecond laser-induced plasma-assisted ablation to create high-aspect-ratio crack-free holes on sapphire substrates (Fig. 2(a)).[36]

The uniformity and surface accuracy of the fabricated structure by wet etching will be affected to a certain extent *via* corrosion. Also, dry etching has limited application range and slow ablation efficiency under vacuum.

Picosecond laser etching and femtosecond laser etching employed in a laser generation system are different, but the steps and auxiliary mode are the same.[37,38]

In the case of laser etching, due to the Gaussian distribution of the laser beam, the temperature distribution of the irradiated point area is also approximately Gaussian distribution, and the temperature of the center area is much higher than the temperature of the edge, which will cause different reactions of substances in different areas. By choosing an appropriate power to match the temperature threshold of the object, the size of the etched hole is smaller than that of the laser spot, which is the reason for the machining resolutions of laser etching beyond the diffraction limit.[39]

2.1.2 Direct laser writing based on two-photon polymerization. Femtosecond laser direct writing (FLDW) based on two-photon polymerization (also known as laser 3D printing
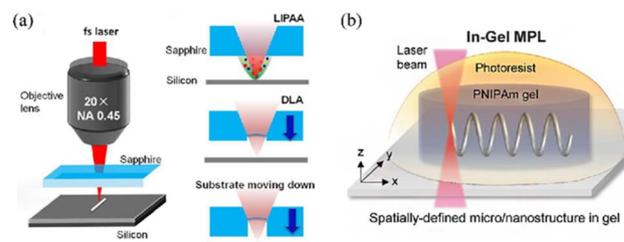

Fig. 2 (a) Schematic of the experimental setup for the fabrication of high-aspect-ratio microstructures on sapphire.[36] Reproduced with permission from ref. 36. Copyright 2020, ELSEVIER. (b) Schematic illustration of in-gel direct laser writing process.[40] Reproduced with permission from ref. 40. Copyright 2018, Wiley.

© 2022 The Author(s). Published by the Royal Society of Chemistry

technology, TPP) is an important micro/nano technology for the manufacture of 3D structures based on the two-photon absorption effect. This technique employs femtosecond laser pulses to make the transition from the ground state to excited state occur by an electron simultaneously in a photosensitive polymer absorbing two photons at a tiny focused volume. The type of modification depends on the nature of the photoresist.[41] For a negative photoresist, due to the cross-linking reaction of the exposed part, which will make it not be dissolved in the developer, and the exposed part remains. Alternatively, for a positive photoresist, laser irradiation will cause the polymer chain to be degraded and broken, which can make it dissolve in the developer, and thus the non-exposed part is reserved after development. Between them, the negative photoresist is the most commonly applied TPP photoresist, which is mainly composed of a photoinitiator to generate free radicals and a crosslinking agent resistant to the developer.[42,43] The developer can be methanol for a conventional photoresist or ethanol for hydrogel. Furthermore, the FLDW processing system usually contains a Ti:sapphire laser and combination of a polarization beam splitter cube and a $\lambda/2$ wave-plate to adjust the laser power.[44]

TPP, a new approach, makes a big difference to 3D micro/nano structuring, owing to its characteristics of nonlinear absorption, high resolution and the universality of objects. The occurrence of TPP only proceeds under laser with high intensity, and also polymerization is triggered only at the focal point of the laser beam, without affecting other regions. This feature enables two-photon laser direct writing technology to achieve the high-precision processing of 3D micro/nano structures, but its point-by-point processing speed is low. Femtosecond projection two-photon lithography (FP-TPL) has been investigated for layer-by-layer printing, ensuring simultaneous temporal and spatial focusing of ultrafast light and leading to an increase in the writing speed.[45]

TPP can achieve spatial resolution below the diffraction limit of laser wavelength, which can be achieved by few-cycle laser pulse.[42] In addition, TPP also has the universality of processing materials, which has gradually expanded from ordinary photoresist to polymethyl methacrylate (PMMA),[46] polystyrene,[47] polytetrafluoroethylene,[48] hydrogels[40,49–53]

(Fig. 2(b)), *etc.* These characteristics are beneficial for the wide applications of TPP.

2.2 Optimization of processing efficiency

Ultrafast laser processing has significant advantages in micro/nano fabrication mainly due to the characteristics of ultrashort pulse and extremely high peak power. Compared with long pulse laser (such as nanosecond laser), the HAZ formed by ultrafast laser processing is ultra-small, and thus the processing quality is sharply improved. However, although ultrafast laser processing has excellent merits, it still faces the problem of low processing efficiency, resulting from the issues associated with the laser and the processing method. Important achievements have been made in optimizing ultrafast laser machining (Table 1).

Nowadays, ultrafast laser is receiving significant attention in industrial applications, where one of the key problems to be solved is its low processing speed, which should be improved, while its processing quality should be maintained. The processing speed is low because of the contradiction of a lower pulse energy and anabatic HAZ due to the increase in the repetition rate. The single pulse energy is relatively low, and thus the repetition rate needs to be improved to obtain an increased processing speed, but this will make the superposition of heat from a continuous single pulse, thereby increasing the formation of HAZ. Therefore, there are two methods to improve the processing speed, while ensuring the quality of ultrafast laser processing. One is to increase the single pulse energy of the laser and the other is to develop a laser that does not increase the HAZ even if it has a high repetition rate.

2.2.1 Increase in repetition rate. GHz laser has shown great potential in improving the machining speed, while ensuring the machining quality. In recent years, it has been found that the temperature drops significantly due to ablative cooling at the repetition rate of GHz. Kerse *et al.* experimentally demonstrated that the very high repetition rate of ablative cooling decreases the laser pulse energy required for ablation and increases the processing efficiency by order of magnitude compared with the previous one.[54] They also provided the direction for clinical ultrafast laser surgery by performing laser ablation on human teeth and brain tissue. Researchers developed related devices for GHz lasers. For example, Bonamis *et al.* reported an easy-to-

Table 1 Various strategies to increase the repetition rate and pulse energy[a]

	PRF	E_{out}	P_{out}	$\Delta\tau_p$	P_{peak}	Ref.
GHz amplified femtosecond laser source	0.88, 1.76, 3.51 GHz (intraburst repetition rates)	—	20 W	<550 fs	—	55
Inscribed thulium waveguide laser (Cr^{2+}:ZnS saturable absorber)	8 kHz	6.9 μJ	55 mW	2.6 ns	2.66 kW	56
Solid-state burst mode amplified laser source	65 MHz (MHz burst mode), 2.5 GHz (GHz burst mode)	—	—	—	—	57
Thin-rod Yb:YAG amplifiers	—	2.5 mJ	28 W	—	—	58
Ultrafast fiber laser	—	12 mJ	700 W	262 fs	—	59
Picosecond optical parametric oscillator	10 kHz	30.5 μJ	—	—	—	60

[a] PRF: pulse repetition frequency, E_{out}: pulse energy, P_{out}: average output power, $\Delta\tau_p$: pulse duration, and P_{peak}: peak power.
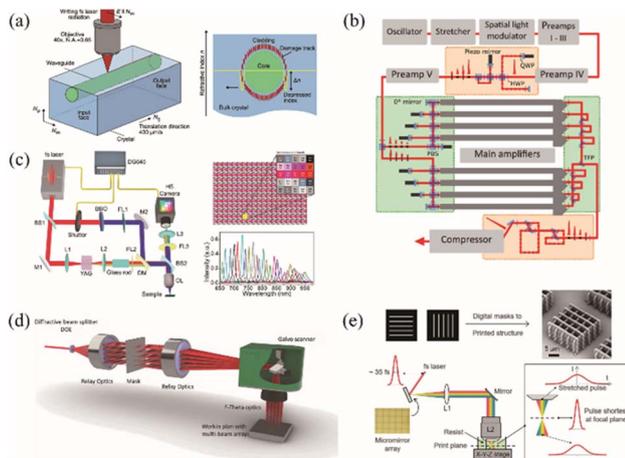
Fig. 3 (a) Femtosecond direct laser writing of channel buried waveguides in a bulk Tm^{3+}:$KLu(WO_4)_2$ crystal and illustration of the geometry of a depressed-index waveguide with a circular cladding (type III structure, end-facet view).[56] Reproduced with permission from ref. 56. Copyright 2020, ELSEVIER. (b) Schematic setup of the eight-channel, four-pulse-replica FCPA system.[59] Reproduced with permission from ref. 59. Copyright 2016, The Optical Society of America (OSA). (c) System configuration of CSMUP for femtosecond laser ablation measurement, filter arrangement on the CMOS sensor in the hyperspectral camera and spectral responses of 25 bands in the hyperspectral camera.[77] Reproduced with permission from ref. 77. Copyright 2021, the American Chemical Society. (d) Principle of generating a static multi beam array.[75] Reproduced with permission from ref. 75. Copyright 2021, IOP Publishing. (e) FP-TPL based on spatial and temporal focusing.[45] Reproduced with permission from ref. 45. Copyright 2019, American Association for the Advancement of Science.

use GHz amplification femtosecond laser source and used it to perform ablation experiments on copper, aluminium (Al), and stainless steel.[55] Kifle and co-workers reported the first watt-level ultrafast laser engraved thulium waveguide (WG) lasers, which is expected to be applied in compact GHz mode-locked lasers (Fig. 3(a)).[56] Metzner and co-workers reported a solid-state pulsed mode amplification laser source with an intra-burst pulse repetition rate of 65 MHz and 2.5 GHz.[57]

The research on the GHz laser and burst mode is still in progress. Bonamis et al. emphasized the importance of experimental parameters to determine the optimal conditions of burst.[55] Although the effect of the GHz laser on improving the processing speed is remarkable, due to the complexity of the heating/cooling balance ablation mechanism, these parameters are still being explored.[55]

2.2.2 Increase in pulse energy. The peak power of the laser is calculated using the pulse energy and pulse width, and the average power is equal to the pulse energy multiplied by the repetition rate. The smaller the pulse width and the higher the pulse energy, the higher the peak power. If the single pulse energy of the laser can be improved, the processing speed will be improved.

An ultrafast laser with a high average power (>100 W) and a high pulse energy (>1 mJ) is required in many practical applications.[58] This requires a reliable and compact laser

source. Fiber lasers have remarkable advantages in terms of reliability; however, the peak power cannot be obtained due to the nonlinear effects in the fiber. Ultrafast fiber lasers usually emit ultra-short pulses with a pulse energy on the nJ level, and their average power is less than 100 mW.[58] Many studies have been carried out to realize fiber lasers with a high average power and high pulse energy. Kienel et al. proposed an ultrafast, high-energy and high-power fiber-chirped-pulse-amplification (FCPA) system with a multi-dimensional amplification structure.[59] Femtosecond pulses with an average power of 700 W and a maximum pulse energy of 12 mJ were obtained using four pulse replicas and eight amplifier channels.[59] The performance demonstrated by the system reveals the great potential of the multi-dimensional amplification concept, which allows the full advantage of fiber optics, while mitigating its limitations (Fig. 3(b)).[59] He and co-workers proposed a novel method for realizing a high-energy ultrafast optical parametric oscillator (OPO) using regenerative amplifier cavity pumping.[60] It was proven that the pulse energy reaches 30 μJ when the pulse repetition rate is 10 kHz and the pulse width is 7.0 ps.[60] This is the highest pulse energy of an ultrafast laser OPO to date.[60] Kuznetsov et al. reported an ultrafast laser system with a high pulse energy (2.5 mJ) and high average power (28 W) based on a unique thin-rod gain module.[58]

Chirped pulse amplification (CPA) or optical parametric CPA (OPCPA) based on laser amplifiers has greatly increased the peak power of lasers by up to megawatts.[61] Quasi-parametric CPA (QPCPA), as a new scheme, has the characteristics of high signal efficiency, wide bandwidth and high anti-phase mismatch ability. It achieves efficient amplification of the chirped signal pulse by exhausting the idle pulse, without the need for reverse conversion.[62–64] Yin et al. demonstrated that QPCPA would break the average power barrier caused by thermal constraints.[61] QPCPA has been shown to be robust to thermal degradation by blocking post-conversion effects.[61] Numerical simulation demonstrated that the QPCPA based on an Sm:YCOB crystal supported a peak power of 3 TW, at 5 kHz and 13 kHz. It was 5 PW at the frequency of 1 Hz, and the average power exceeded 150 W in both cases.[61]

2.2.3 Other optimization methods. Other optimization methods mainly solve the issues of low efficiency and poor mechanical strength in ultrafast laser processing based on realizing ultra-high machining accuracy. These methods can optimize ultrafast laser processing to a certain extent. Also, although they exhibit various problems, these methods are undoubtedly an important research direction to improve the efficiency of ultrafast laser processing.

Femtosecond laser TPP (FL-TPP) is undoubtedly an important method to achieve 3D micro/nano machining, while near-threshold processing is considered as an indispensable strategy in FL-TPP, which can achieve ultra-high machining accuracy but has the problems of insufficient structural mechanical strength and long processing time. Several solutions have been proposed to overcome these problems. For example, Gross et al. proposed a post-processing method using oxygen plasma to improve the performance of TPP.[65] They found that using octahedral micro lattices as a temporary

support could prevent its movement during exposure, stabilize the beam during development, and most importantly, move it out after 25 min of exposure to oxygen plasma.[65] They made a flawless flower using this method, which possessed a stem of 3.75 ± 0.12 μm and petal thickness of 1.5 ± 0.1 μm.[65] It was proved that fine and complex structures can be produced by this method. To shorten the processing time, parallel multi-focus and focal field engineering (FFE) have also been proposed.[65] Geng et al. proposed a novel laser nanomachinery process based on TPP and an ultrafast random-access digital micromirror device (DMD) scanner.[66] This method expands single-focus scanning to parallel multi-focus scanning.[66] The DMD scanner has unique advantages in precisely controlling the laser dose and focus position (~100 nm).[66] Therefore, it can be employed to design and manufacture complex 3D structures.[66] Yang and co-workers firstly demonstrated 3D microstructures by a single-exposure TPP based on 3D FFE.[67] Hu and co-workers proposed the DRS processing concept, where D refers to the use of low-power near-threshold femtosecond lasers and R refers to the high-power femtosecond laser enhanced scanning of the inner surface of structures.[68] S represents irradiating internal unpolymerized materials by continuous ultraviolet (UV) light.[68] Combining these three steps, the problems of low processing efficiency and mechanical strength can be effectively solved in near-threshold TPP.[68]

The spatial shaping of ultrafast lasers also has an important impact on the processing efficiency. The cross section of the laser beam emitted by the traditional laser is usually a Gaussian profile. When an object with a special shape is processed by this way, point scanning is needed, which puts forward high requirements for the quality and accuracy of the laser spot. Beam space shaping can directly complete the machining of microstructures with various shapes under the exposure of single or multiple pulses, thus improving the machining efficiency and resolution.[69,70] In addition, it can be applied to single-step machining of special spatial contour microstructures,[71] high-depth-aspect ratio structures,[72,73] microarray structures and high-quality machining of various cross-scale hierarchical structures.[74] Luo et al. proposed a method to process high-quality cylindrical microlens arrays (MLAs) on the surface of quartz glass through femtosecond laser shaping technology.[71] They spatially fitted a Gaussian laser beam into a Bessel beam to obtain an anti-cylindrical laser intensity distribution in a specific section of the light field.[71] The numerical simulation results showed that the envelope of light intensity distribution of this shape is consistent with the required morphology of cylindrical microlens, and the cylindrical MLA can be directly fabricated by line scanning of the shaped femtosecond laser on quartz glass.[71] Furthermore, the radius and depth of the microlens element can be controlled by adjusting the laser power.[71] Xie and co-workers used a femtosecond laser Bessel beam to control the local transient spatial electron density and performed single pulse processing of high-aspect-ratio and high-quality micropores in PMMA.[72] The quality of the processed microholes at the entrance and side walls was higher than that of the microholes processed by a Gaussian beam.[72] The aspect ratio of a microhole by

femtosecond laser Bessel beams can be up to $330 : 1$.[72] Roth et al. adopted adaptive beam shaping technology and used a femtosecond laser to process microchannels with almost no length limitation inside PMMA.[73] They used a spatial light modulator (SLM) to compensate for the writing depth determined by spherical aberration, resulting in a precisely controllable and stable cylindrical shape.[73] Hu and co-workers employed holographic FLDW technology to prepare aspheric microlens arrays (AMLAs) in parallel.[74] In this process, they considered the inherent characteristics of SLM and compensated the defects of multi-focus mode to obtain higher intensity uniformity and optical efficiency.[74]

In laser ablation, Finger et al. reported a method for treating an arbitrary surface with high quality and efficiency, and they proposed a system that can use an average output power of 1 kW with fs pulse duration (Fig. 3(d)).[75] Žemaitis and co-workers compared two methods for optimizing laser ablation efficiency, using optimal parameters for rapid ablation and 3D machining.[76]

In addition to the above-mentioned methods, Saha et al. developed FP-TPL technology to realize parallel printing of arbitrary complex 3D structures with sub-micron resolution (Fig. 3(e)).[45] Yao and co-workers reported a chirped spectral mapping ultrafast photography (CSMUP) system for single real-time ultrafast imaging of femtosecond laser processing by combining femtosecond laser processing with visualization and imagination.[77] This method proposed a new strategy for improving the accuracy and efficiency of femtosecond laser processing (Fig. 3(c)).[77]

3   3D micro/nano structures by ultrafast laser

Because it involves few steps, no mask, fast processing and is environmentally friendly, ultrafast laser is widely applied in many fields, resulting in the birth of a variety of ultrafast laser-processed structures. The size of the structures ranges from 100 μm to submicron.[21,78–84] In this section, we review a variety of 3D micro/nano structures fabricated by ultrafast laser, including porous structures, grooves, channels, arrays and nets.

3.1   Porous

As a common 3D structure, micro/nano porous structures are widely used in microsensors, aircraft turbine blades, nuclear fusion structures, microelectrodes, oil-water separation, etc.[85,86] Although porous structures have been reported by many researches, and various porous structures studied, the processing on different materials, as well as the fabrication of pores with a high ratio of depth to diameter, and the blind holes with taper face great challenges.

The quality, precision, and depth of ultrafast laser drilling rely on the material. Drilling in alloys is common.[87–90] Zhai et al. drilled holes with an inner diameter of 162 μm, an aspect ratio of $15 : 1$ and almost zero taper on nickel-based alloy with thermal barrier coatings.[89] Furthermore, they claimed that the depth and diameter of hole increased linearly with an increase

in the pulse number.[89] The self-focusing effect of femtosecond laser drilling has an important effect on the quality of deep holes. Wang and co-workers reported that the self-focusing effect has a regulating effect on enhancing the laser intensity in the cavity and a great influence on strengthening the intensity of microhole during the drilling process, which is not associated with the aperture.[91,92]

In addition to alloys, ultrafast laser drilling can be performed on polymers, ceramics, glass and other materials.[82,93–96] Liu and co-workers fabricated an all-silicon uniform-aligned concave MLA through dry-etching-assisted femtosecond laser machining.[34] Jiao *et al.* proposed a new method for applying a direct current to a silicon substrate during picosecond laser drilling.[97] Because the voltage applied externally causes the free electrons to behave in a more orderly manner, it increases the current flow in the silicon substrate and enhances the energy absorption of silicon by laser. Besides the ultrafast laser drilling techniques adopted in different materials, some relatively general ultrafast laser drilling techniques also exist.[98]

Incredibly, Wang and co-workers processed holes on PMMA.[94] In this study, an axial-hole lens with different cone angles was used to transform the incident Gaussian beam into a Bessel beam with different non-diffraction lengths and focus on the sample for processing. The aspect ratio of micropores was enhanced by increasing the pulse number and the cone angle of the axial cone lens. This method achieved the maximum ratio of depth to diameter of micropores (348 : 1).[94]

In addition, ultrafast laser processing of porous has a self-cleaning effect, that is, the molten spatter after ultrafast laser etching is removed with continuous laser irradiation. Zhao *et al.* studied surface morphology and internal morphology based on the self-cleaning effect (Fig. 4(a)).[78] Mishchik and co-workers indicated that when the focused numerical aperture is in the range of 0.08 to 0.15, the removal efficiency of dust is the highest when the holes are processed on sapphire.[99]

3.2 Groove and channel

Groove structures are important common structures in micro/nano devices. The most representative ones are microfluidic channels applied in the biomedical field, micro/nano grating applied in the optical field, trench-like microelectrode applied in the electrochemical field, *etc.*[100,101] Therefore, the machining of micro/nano grooves is of great significance. Laser engraving is currently the most common method of manufacturing.

The working principle is similar to that of ultrafast laser drilling described in Section 3.1. Fig. 4(b) describes the glass micro channel fabricated by femtosecond laser combined with wet chemical etching.[21] Also a silver film was placed on the wall of helical hollow microchannels. Moreover, different features were obtained in channel structures on different materials by ultrafast laser processing. For the grooves prepared on Al-doped silicon carbonitride (SiAlCN) ceramics, the number of femtosecond laser scans and the energy fluences will affect the quality of the grooves. Chen *et al.* pointed out that when the energy fluences increase, the ablation is serious and a HAZ is generated, resulting in low machining quality.[79] However, increasing
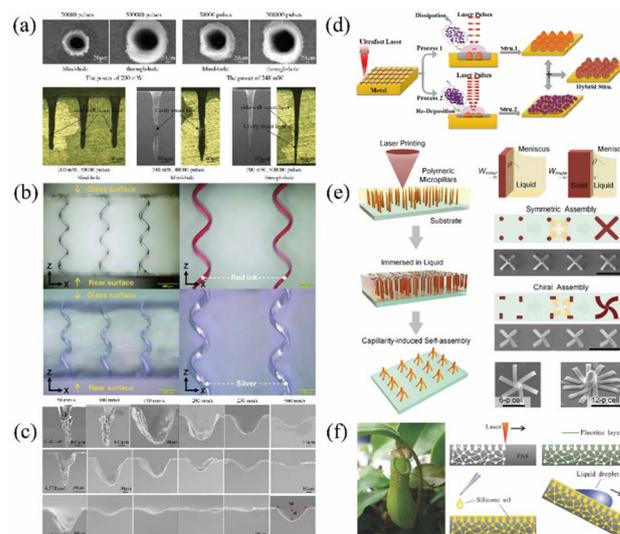

Fig. 4 (a) SEM images of holes surfaces (wavelength: 1064 nm) and categories of the recast layers inside the holes based on the location (wavelength: 1064 nm).[78] Reproduced with permission from ref. 78. Copyright 2018, Elsevier. (b) 3D helical microchannels.[21] Reproduced with permission from ref. 21. Copyright 2018, Wiley. (c) Cross-section SEM microphotographs of the laser-machined grooves fabricated with different scan speeds at three certain energy fluences (1.14, 4.57, and 11.43 J cm^{-2}). Inserted in the lower right corner: definition used herein for the width (*W*) and depth (*d*) of the grooves.[79] Reproduced with permission from ref. 79. Copyright 2020, Elsevier. (d) Schematic illustration of the pulse injection controlled ultrafast laser direct writing strategy.[80] Reproduced with permission from ref. 80. Copyright 2017, the American Chemical Society. (e) Preparation of deterministic chiral structures by combining laser printing and capillarity-induced self-assembly.[81] Reproduced with permission from ref. 81. Copyright 2020, Wiley. (f) Process of preparing a slippery liquid-infused porous surface (SLIPS) by FLDW.[82] Reproduced with permission from ref. 82. Copyright 2017, Wiley.

the scanning speed at the same energy fluences will decrease the removal rate and ablation degree. Also, the HAZ is associated with both the scanning speed and energy fluences. Laser parameters with a high scanning speed or low energy flux are helpful to avoid the formation of HAZ on SiAlCN ceramics.[79] The results demonstrated that a scanning speed above 250 mm s^{-1} and energy flux below 4.57 J cm^{-2} are beneficial for the manufacture of high-quality grooves.[79] Fig. 4(c) shows the influence of scan speed and energy on the laser-machined grooves. Grooving polyether ether ketone (PEEK) is widely applied to prevent bone formation.[102] During this process, the femtosecond laser can form micro grooves and nanometer-scale pore clusters on the surface of the material, both of which have an obvious synergistic effect. The groove has a great correlation with the appearance of grooves and pore clusters. The results indicated that at the spacing of 2 μm, the surface of the processed material had a great amount of irregularly distributed pore clusters but no regular periodic grooves. When the widths of the surface groove of PEEK were 10 and 15 μm, the spine of the groove was also covered by nanopore clusters. In addition to making biomimetic bone, it also has an important role in the cluster and differentiation of osteoblasts.[103]

3.3 Array

Array structures enable structural or functional units to have special functions, such as anti-reflection,[80,104–106] anti-icing,[107,108] and electron emission.[109] The array structure can also be used to obtain an increased specific surface area. However, the preparation of the array structures requires complicated steps, some of which cannot be achieved by traditional methods. Femtosecond laser processing can simplify the process and improve the preparation efficiency.

For a surface with a special function, femtosecond laser processing can be applied to improve the preparation efficiency. For special functional surfaces that have anti-reflection performance, Wang et al. employed the femtosecond laser texturing technique to fabricate quasi-uniform cone-array microstructures on single-crystal silicon directly.[104] The structure has a peak depth of up to 8 μm, which significantly reduces light reflection. Compared with planar silicon wafers, the relative reflectance of the cone array decreases to less than 9% in the measurement wavelength range (400–1000 nm). Fan and co-workers proposed and experimentally demonstrated a universal pulse injection-controlled ultrafast laser direct writing method for the fabrication of highly efficient antireflective structures on the surface of metals (Fig. 4(d)).[80] By this method, the obtained minimum reflectance of the UV-NIR wideband spectral region on Cu, Ti, and W surfaces were 1.4%, 0.29%, and 2.5%, respectively.[80] The proposed method is easy to access, suitable for different types of metals and large-area production, with double-scale characteristics. Li et al. fabricated an inverted pyramid and cone array with a pitch of about 2 μm and a total height of nearly 900 nm using an FLDW assisted by wet etching.[105] The transmittance measurements between 3 μm and 5 μm were consistent with the simulation results using VirtualLab, and the transmittance reached a maximum of 92.5% at 4 μm.[105] Liu and co-workers developed a collaborative 3D micro/nano manufacturing method using femtosecond laser and oxidation technology.[106] They fabricated the conical structure of a uniformly loaded nanowire, namely, an urchin-like structure.[106] This method was experimentally verified to be environmentally friendly and has no toxicity.[106] In addition, the reflection test of the constructed sea urchin-like array demonstrated the excellent anti-reflection performance in the ultra-wide spectrum of UV, visible, infrared and far-infrared (FIR), which was fully realized on the surface of copper.[106]

For special functional surfaces that have anti-ice performance, Jiang et al. proposed a technique to prepare layered micro/nano structures on the surface of metals by high-temperature stamping with a mold by ultrafast laser ablation.[107] The surface structure of the prepared copper was hydrophobic, which became superhydrophobic after chemical modification.[107] This method combines the advantages of ultrafast laser ablation to fabricate a micro/nano mold with high-temperature lithography to obtain a micro/nano structure on the surface of the target metal.[107] Pan and co-workers designed and fabricated a novel triple-scale micro/nanostructured superhydrophobic surface, with excellent ice-phobic and anti-icing performance.[108] The surface was fabricated by chemical oxidation and ultrafast laser ablation.[108] Also, it had excellent Cassie state stability and the critical Laplace pressure was up to 1450 Pa.[108] Its ice adhesion strength had a low value of 1.7 kPa.[108]

For a special functional surface capable of electron emission, Xiao et al. fabricated a field emission array of single-crystal lanthanum hexaboride (LaB_6) with uniform mountain emitter morphology using a UV femtosecond laser at a high speed.[109] The height of the mountain emitter was 6 μm and the radius of the curvature was 100 nm.[109]

Array structures can also be employed to increase the surface area of active electrodes. Femtosecond laser processing can simplify this process and improve the preparation efficiency. Cui and co-workers developed a highly effective method to fabricate manganese oxide directly on the surface of a 3D manganese collector.[110] In their process, a 3D conductive network on the surface of manganese was generated by a femtosecond laser and the network also acted as a current collector (named 3D Mn).[110] Manganese oxides were then directly formed on the femtosecond laser-structured surface by chemical oxidation (named 3D Mn/MnO_x).[110] This structure had a large specific surface area, which shortened the transport path of electrons/ions, promoted electrolyte penetration, and reduced the contact resistance between 3D Mn and MnO_x, which are conducive to long-term electrochemical cycling.[110] Kwon et al. proposed a laser direct writing technique based on TPP for the fabrication of a photoresist-derived carbon cross finger electrode (PRC-IDE) with a large areal capacitance.[111]

In addition, femtosecond laser processing has extremely high preparation efficiency compared with other commonly used fabrication technologies. Hu et al. combined femtosecond laser printing with capillary-induced self-assembly to obtain a mesoscale chiral architecture with high designability and customizability (Fig. 4(e)).[81] They took advantage of the flexibility of femtosecond laser printing to achieve a variety of chiral assemblies.[81]

3.4 Net

The net structure fabricated by femtosecond laser processing is a type of unique 3D structure, which also has some novel functions.

Regular net structures such as cell scaffolds are processed by TPP. For example, Heitz et al. processed three-level pentaerythritol triacrylate (PETA):bisphenol a glycidyl methacrylate (BisGMA) cage structures by TPP on polyethylene terephthalate (PETG) substrates, which were used to fill bone-forming cells and generate 3D mineralized protein networks.[112] Trautmann and co-workers adhered human primary fibroblasts to scaffolds prepared by TPP.[113]

Irregular net structures such as porous networks have been proposed. Yong et al. directly formed a 3D porous network structure on a polyamy-6 (PA6) substrate and tested a variety of liquids for their repellency (Fig. 4(f)).[94] These liquids include water, cetane, lake water, ink, glycerin, coffee, milk, egg whites and egg yolks.[94] In 2018, Yong and co-workers employed one-

step FLDW to prepare porous network microstructures on the surface of various polymers.[93] They also found that the growth of C6 glioma cells was promoted by the original laser-induced porous PET surface as a culture substrate, while the smooth surface of PET completely inhibited the growth of C6 glioma cells.[93] As another type of irregular networking structure, the carbon nanoribbon network (CNRN) platform plays an important anti-cancer role. Chowdhury *et al.* developed a CNRN platform bottom-up by femtosecond laser ionization.[83] They transformed an abiotically reactive graphite matrix into a bioactive interwoven CNRN platform.[83] Their experiment proved two distinct simultaneous functions of the CNRN platform, *i.e.*, the attractive properties of the extra cellular matrix (ECM) and the therapeutic properties without the need to bind any biomolecules/drugs.[83] The CNRN platform contributes to enhancing the cellular attractiveness and selective functions, enabling fibroblasts to exhibit tissue-like behavior and HeLa cells to perform apoptosis-like functions.[83] Huang and co-workers successfully prepared a precise 3D scaffold with living cell encapsulation using the TPP technique, and no obvious cell damage was observed during the manufacturing process.[114] The advantages of laser processing for different structures are summarized, as shown in Table 2.

4 Micro/nano devices based on 3D structure

4.1 Turbine blades

Aircraft turbines can work at thousands of degrees (°C). Therefore, these high-temperature devices must have excellent cooling capacity. On the microscopic scale, aircraft turbine blades (including alloy structure, blade core and thermal barrier coating) always have the arrangement of a large number of micropores, which is a typical application of pore structures.

For alloy structures on the outside of the blade, the treatment of high-quality hole structures on the turbine blade often utilizes ultrafast laser ablation. However, a more thorough understanding of the interaction between the laser and material during machining is required. The interaction can be based on the traditional two-temperature model.[115] Besides, some studies analyzed the ground laser ablation of Ti_6Al_4V alloy using the two-temperature model and proposed the multi-pulse ablation method, which further improved the quality of processed holes.[116] This two-temperature model is based on a set of

coupled partial differential equations in the time and space domain.

In addition to the alloy blades, there are blade cores and thermal barrier coatings. The core of the turbine blade is typically porous alumina ceramic and its cavity plays an important role in the service life and performance of the turbine blade. Min and co-workers investigated the femtosecond laser treatment of porous alumina ceramics.[117] They studied gas-assisted and water-assisted processing methods and determined the optimal working window of processing. For drilling a thermal barrier coating on turbine blades, Wang *et al.* performed drilling on the thermal barrier In718 coat using a femtosecond pulsed Ti:sapphire laser.[118] Also, they analyzed the influence of the polarization of the laser beam on microhole profile and morphology of periodic structures on the sidewall of microhole.[118] They found that with circular polarization, the periodic structure had a ball-like profile. Alternatively, under linear polarization, periodic structures of pine needle-like type were obtained.[118]

4.2 Micro energy devices

In recent years, there has been remarkable development in micro/nano electronic devices, and the emergence of micro/nano sensors, micro/nano robots, micro/nano actuators and flexible wearable devices also pose great challenges in the power supply.[119,120] To meet the demand for power sources, micro energy devices must have a sufficient energy density. Thus, in the case of the manufacture of micro energy devices, the design, choice and treatment of materials with special structures become a critical issue, and therefore highly suitable and effective machining process is required.[121-124] At present, most of the ultrafast laser processing of 3D structures applied in micro energy devices involves two approaches.

One is the formation of active microelectrodes and composite microelectrodes by laser etching.[125-127] Zheng *et al.* processed line and grid structures layer-by-layer on silicon/graphite (Si/C) electrodes.[125] These two microstructures provided more free space for volume changes, and the mechanical stress of the electrode was reduced. Furthermore, the fabricated graphite electrode delivered an excellent high rate capability up to 3C beyond state-of-art cells. This processing is faster than those of other methods for the manufacture of microelectrodes. Kurra and co-workers described in detail the laser processing of 3D graphene electrodes.[126] He *et al.*

Table 2 Summary of the advantages of laser processing for different structures

	Structural features	Ultrafast laser processing methods	Advantages of laser processing	Ref.
Porous	Better surface topography and much deeper	Ablation	Self-cleaning effect, short pulse duration and high peak power	78 and 89
Groove and channel	High ratio of depth to diameter	Ablation and laser direct writing (LDW)	Excellent thermal stability, short pulse duration and high peak power	99
Array	Rational alignment	Ablation and LDW	High speed	—
Net	Complex and 3D	LDW	High resolution	21

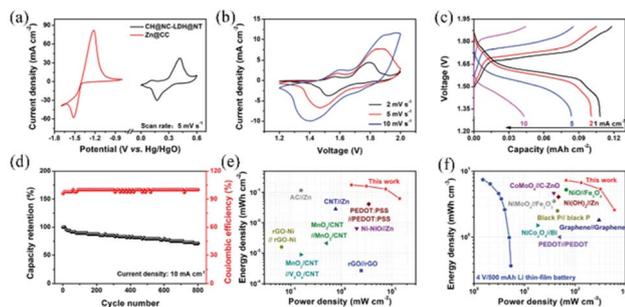**Fig. 5** Electrochemical performances of Co–Zn micro-battery. (a) Cyclic voltammetry (CV) curves of $Co(OH)_2$@NiCo-layered double hydroxide@Ni-coated textile and Zn@carbon clothes at 5 mV s^{-1}. (b) CV curves, (c) galvanostatic charge−discharge (GCD) curves, (d) long-term cycling stability, and (e and f) Ragone plots of Co–Zn micro-battery.[127] Reproduced with permission from ref. 127. Copyright 2020, Wiley.

fabricated a high-performance in-plane Co–Zn alkaline micro-battery by laser dry etching. Fig. 5 shows the electrochemical performance of the fabricated Co–Zn microbattery.[127]

The other approach is the use of LDW technology of TPP.[128–130] Most processes are conducted for the treatment of polymers. For example, Staudinger *et al.* manufactured conductive microstructures on carbon nanofiller absorbers using this technology.[128]

4.3 Microfluidics

Microfluidic devices consist of a series of channels or chambers containing and manipulating fluid with ultra-small volume. They have been widely used in the biomedical field due to their high throughput, single-cell resolution and mixing efficiency.[131] Since their appearance in the 1990s, microfluidic devices have been developing towards miniaturization and integration, which require high precision, high resolution, low cost and mass production for their manufacture. Ultrafast laser machining is emerging as a powerful process for the large-scale manufacturing of microfluidic devices, especially for devices with complex structures. For instance, laser wet etching technology was used in fused silica to obtain 3D microcoils,[12] and Fig. 6(c) describes the process of filling 3D microcoils with metal gallium in fused silica.[132]

TPP technology is used in processing polyethylene glycol-based hydrogels and protein-based biomolecules.[133] To apply FLDW technology in the fabrication of 3D channels in glass, and then remove the glass matrix by HF, as similar as the procedure by Xu *et al.*,[21] TPP and femtosecond-laser-assisted wet etching (FLWE) hybrid femtosecond laser processing can also be applied.

In the study by Wang and co-workers, "all-in-one" femtosecond laser processing was adopted to obtain multilayer microfluidic channels, and Fig. 6(a) shows their fabrication procedure.[134] To create microchannels with high quality and uniformity, they optimized the power density of the laser. Fig. 6(b) demonstrates an eight-layered microfluidic chip integrated with the fabricated polymer microstructures. Wang *et al.*
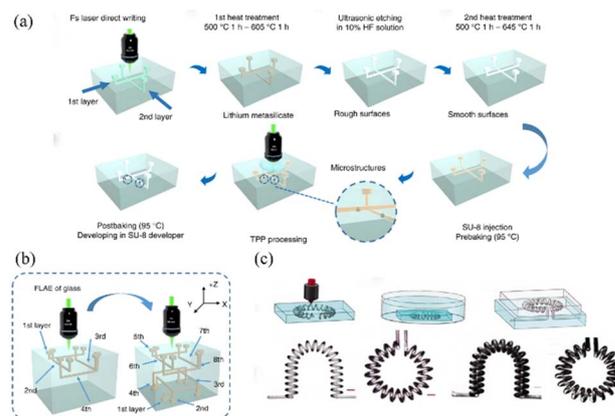

Fig. 6 (a) Schematic illustration of the procedure for the fabrication of 3D multilayered microfluidic chips.[134] Reproduced with permission from ref. 134. Copyright 2019, Springer Nature. (b) Schematic illustration of the process for the fabrication of eight-layered glass microchannels by femtosecond laser.[134] Reproduced with permission from ref. 134. Copyright 2019, Springer Nature. (c) Schematic of the two-step fabrication process and different shapes of microchannels and inductances.[132] Reproduced with permission from ref. 132. Copyright 2013, The Optical Society of America.

summarized numerous processing technologies for microfluidic devices.[135]

The slow progress in the treatment of malignant tumors, lack of tumor models and difficulty in simulating the narrow space of tissues and organs during their spread are important reasons that hinder pathophysiological research. Sontheimer-Phelps and co-workers, described in detail the important role of microfluidic devices in cancer treatment.[136] Sima *et al.* processed submicron polymer channels of different lengths by TPP and chemically assisted femtosecond laser etching, which is a novel biochip with 3D polymer nanostructure.[137] Also, they successfully observed the morphological change in cells during migration. In addition to pathological studies in cell cultures, Lao and co-workers produced a microchannel with a nanostructure for the local sensing of anti-cancer drugs (doxorubicin).[138]

Besides, microfluidic systems for applications in cell culture and observation, optical fluidic adaptive imaging and biomedical sensing are attracting attention.[139,140]

4.4 Microlens arrays

In MLAs, their aperture and relief depth are on the micrometer scale. They not only have the traditional lens focus and basic function such as imaging, but also have the characteristics of small cell size and high integration and can form various new optical systems. Nowadays, MLAs are important components in integrated micro-optics systems.

Femtosecond laser processing and wet etching are used to fabricate MLAs. Yang *et al.* fabricated a double-sided concave MLA for generating novel and diverse imaging patterns by FLWE (Fig. 7(a)).[23] Also, Zhang and co-workers employed this method to prepare a large-area concave MLA.[141] They produced about 2 million quasi-periodic MLAs with an adjustable

diameter and depression height within 30 min.[141] Li *et al.* prepared a superhydrophobic polydimethylsiloxane (PDMS) MLA by combining FLDW and FLWE (Fig. 7(b)).[142] The prepared MLA not only had ultra-low adhesion, ultra-high hydrophobicity and excellent imaging performance, but also had excellent water resistance and self-cleaning function compared with ordinary MLAs.[142] Cao and co-workers prepared hard templates using a combination of femtosecond laser processing and wet etching, and prepared soft and thin PDMS MLAs through soft etching (Fig. 7(c)).[143] Instead of making MLAs directly, they made silicon templates, which could then be used to obtain large-scale, highly homogeneous PDMS MLAs *via* soft lithography.[143]

Furthermore, MLAs can also be prepared by femtosecond laser and ion beam etching. Liu *et al.* applied this method to prepare nanosmooth MLAs on rigid materials (such as molten quartz, gallium arsenide, silicon carbide and diamond) in a convenient and multifunctional way.[144]

4.5 Cell scaffold

Tissue engineering involves the use of cells and scaffolds/ matrices to develop novel functional tissues for implantation into donors. With the great demand for tissues and organs, tissue engineering has developed to create living replacements for body. The need for tissue engineering is further proposed by the widening gap between demand and supply of organs or transplantable tissues. Cell scaffolds are an important component in tissue engineering. Scaffolds provide a favorable environment and support for the attachment and growth of tissue. They can also be applied as a template or carrier for tissue

implantation and drug delivery.[145] At present, the main method for the preparation of scaffolds is 3D printing based on femtosecond lasers.

TPP 3D printing technology based on femtosecond lasers is widely employed. Thompson and co-workers proposed the preparation of a poly (caprolactone) (PCL) scaffold by TPP for human retinal progenitor cells.[146] One month after the implantation of the cell-free scaffolds in pig models of retinitis pigmentosa, there was no infection, inflammation, local or systemic toxicity.[146] Furthermore, comprehensive ISO 10993 tests of the photopolymerized scaffolds showed their high biocompatibility. Wang *et al.* prepared microcapsules *via* the TPP method based on structured laser beams and studied the culture of budding yeast using the microcapsules to demonstrate their application as a 3D cell culture scaffold.[24] Richter *et al.* fabricated 3D scaffolds for cell culture *via* direct laser writing, where the scaffolds had a boxing-ring-like structure (Fig. 8).[147] Song and co-workers reviewed hydrogel scaffolds prepared using TPP, provided an in-depth description on various biological and mechanical characterizations for
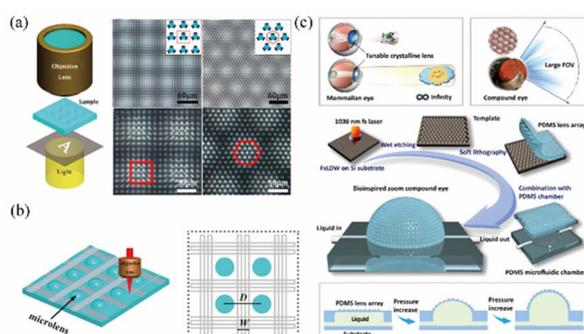

Fig. 7 (a) Schematic illustration of the microscopic imaging system. The bottom side of the MLA observed by the top side of the MLA (insets respectively represent the arrangement of the rectangular-shaped and hexagonal-shaped MLA on each side) and imaging properties of the letter "A".[23] Reproduced with permission from ref. 23. Copyright 2018, Elsevier. (b) Schematic illustration of the fabrication of criss-cross reticular rough structures around the microlenses and top view of as-prepared MLA.[142] Reproduced with permission from ref. 142. Copyright 2019, Wiley. (c) Schematic illustration of the design principles of a variable-focus compound eye, working principles and properties of a monocular eye, and working principles and properties of a compound eye. Schematic illustration of the fabrication process of the zoom compound eye. Regulation principle of the zoom compound eye.[143] Reproduced with permission from ref. 143. Copyright 2020, the American Chemical Society.
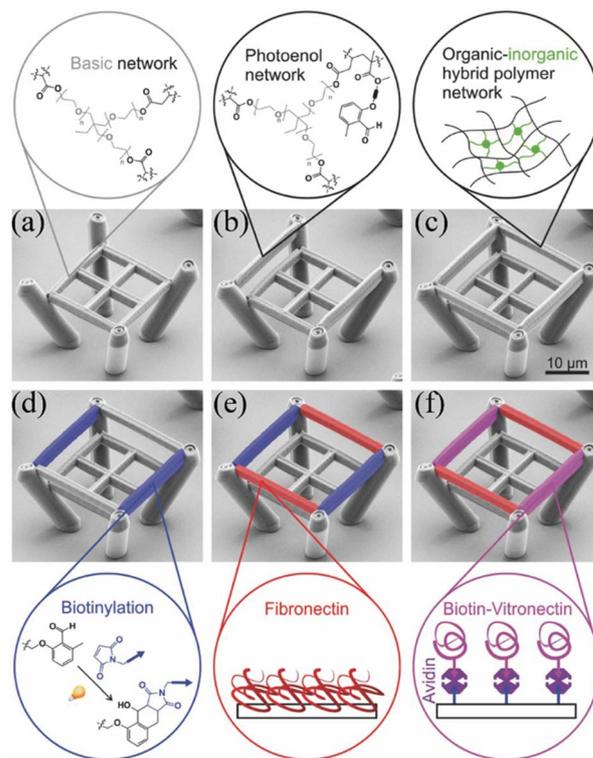

Fig. 8 Pseudo-colored scanning electron microscopy (SEM) images illustrating the sample preparation process.[147] (a) Scaffold produced in the first direct laser writing step using the basic resist. (b) In a second direct laser writing step, two beams of the functional resist (here, photoenol resist) were added to the scaffold. (c) In a third direct laser writing step, two additional OrmoComp beams were written. (d) Post-modification of the resulting microstructure *via* UV light leads to biotinylation of the functional resist (blue). (e) Fibronectin (red) exclusively binds to OrmoComp beams. (f) By subsequent coating steps with avidin and biotin−vitronectin (magenta), only the functional resist is addressed by this extracellular matrix protein. Reproduced with permission from ref. 147. Copyright 2016, Wiley.

evaluating the structures, and described the design requirements for cell and tissue-related applications.[148] Three case studies of bone, cancer and heart tissue were also presented to elaborate the need for structural materials in the next generation of clinical applications.[148]

Cell scaffolds have also been prepared by femtosecond laser and 3D printing. Daskalova and co-workers achieved efficient production and post-processing of biomimetic and biodegradable PCL scaffolds using a combination of femtosecond laser processing and 3D printing.[149] The results demonstrated that the hydrophilicity of PCL materials is improved by femtosecond laser processing.

4.6 Micro/nano robot

In addition to the above-mentioned microfluidic technology, micro/nano robots also have important applications in the treatment of some diseases due to their minimal invasiveness. Because of their micro scale and complex 3D structure, the accuracy and designability of the processing of micro/nano robots are necessary. Thus, ultrafast machining, especially FLDW technology in the fabrication of micro/nano robots is attracting great interest.

Jeon *et al.* fabricated a micro-robot using FLDW, which is powered by a magnetic field and can provide precise positioning.[150] The proposed micro robot was applied to metastasize colorectal cancer cells. Moreover, this FLDW was employed to create smart and deformable 3D micro actuators.[151] Although micro robots show great potential in the medical field, they also face some challenges, especially biocompatibility.[22]

Because traditional laser processing is mostly focused on a single material, artificial organs and tissues cannot be precisely assembled from multiple materials. Ma and co-workers proposed an on-chip TPP strategy for the fabrication of artificial musculoskeletal systems, which also provides the possibility for fabricating various 3D structures.[152] Furthermore, this strategy was preliminarily verified by producing a spider micro robot and 3D intelligent micro claw.

5 Conclusion and perspective

Ultrafast lasers are attractive because of their high power density, ultra-short pulse and extremely high peak power. Thus, due to these characteristics, ultrafast lasers are employed in various fields, ranging from micro/nano sensors, communication and consumer electronic-related components to aerospace. At present, ultrafast laser processing is gaining interest due to its high speed and high precision. The main ultrafast laser processing methods for 3D structures are picosecond laser etching, different auxiliary types of FLDW and femtosecond laser etching based on TPP. In this review, we introduced the principles of ultrafast laser fabrication and the optimization of its processing speed. Especially, the optimization of the repetition rate and pulse energy of laser is of interest. Furthermore, specific pulse intensities and fluences are required in suitable modifications, which are also very important parameters. For instance, the ablation pattern of protein crystals is determined by the pulse number and laser fluence.[153] When the laser fluence is higher

than 1 J cm^{-2}, the protein crystal is directly removed to form the ablation hole.[153] At a laser fluence below the threshold of single-pulse ablation, which was calculated to be $\sim 0.4 \text{ J cm}^{-2}$ for a single pulse, the protein was denatured due to energy deposition. Through the accumulation of multiple pulses, the denatured protein could not maintain its crystal shape and formed a foaming form. Both the ablation pore and the foaming zone contributed to the surface topography of the ablation zone, resulting in unique physical and chemical performances. The nonlinear absorption of protein single crystals is proportional to the m order of the laser intensity, where m is the number of photons absorbed by an electron. The sharpening of the absorption region resulting from the multiphoton absorption is helpful for the ablation region exceeding the diffraction limit with high accuracy.[153] For PMMA, the experimental method is to measure the average laser power delivered to the sample using a calibrated integrating sphere optometer after focusing the focal plane of the lens. The experimental results showed that the threshold fluence is predicted to be 0.97 J cm^{-2} when the number of pulses N is 20. Both the ablation depth and the average roughness of the ablation region increase with an increase in the laser fluence.[154] Afterward, typical 3D structures machined by ultrafast laser, including porous structures, channels, arrays and net structures are elaborated. Also, the applications of these structures in turbine blades, microfluidics, micro energy devices, MLAs, cell scaffolds and micro/nano robots are described in detail. All these 3D structures applied in different devices are of great significance in medicine, energy and optics. The corresponding discussion and summary of these methods as well as optimization for 3D structures will also provide valuable strategies to researchers in future studies.

To the best of our knowledge, ultrafast laser processing is limited by its high cost and immature control technology. Besides femtosecond and picosecond lasers, ultrafast lasers also include attosecond lasers. Attosecond lasers with a big leap in pulse width are expected to be an important driving force in microelectronic devices. At the current state, many studies have explored the interaction between metal micro/nano particles and attosecond laser pulses, achieving fascinating progress. This will promote the applications of attosecond lasers in many fields. Thus, it can be predicted that ultrafast lasers will become the main approach in the field of precision engineering.

Author contributions

P. Tian conceived the idea and supervised the whole study. X. Yang and R. Song wrote the manuscript. X. Liu, L. He, X. He, Z. Ma revised the manuscript. L. Wu, X. Liu, H. Tang, X. Lu helped to collect the information, and edited the figures and tables. All authors discussed the review and assisted during manuscript preparation.

Conflicts of interest

There are no conflicts to declare.

Acknowledgements

References

1 K. C. Phillips, H. H. Gandhi, E. Mazur and S. K. Sundaram, *Adv. Opt. Photonics*, 2015, **7**, 684–712.

2 J. Huang, L. Jiang, X. Li, S. Zhou, S. Gao, P. Li, L. Huang, K. Wang and L. Qu, *ACS Appl. Mater. Interfaces*, 2021, **13**, 43622–43631.

3 S. Bagheri, K. Weber, T. Gissibl, T. Weiss, F. Neubrech and H. Giessen, *ACS Photonics*, 2015, **2**, 779–786.

4 Y. Liu, X. Li, J. Huang, Z. Wang, X. Zhao, B. Zhao and L. Jiang, *ACS Appl. Mater. Interfaces*, 2022, **14**, 16911–16919.

5 J. Huang, K. Xu, J. Hu, D. Yuan, J. Li, J. Qiao and S. Xu, *Nano Lett.*, 2022, **22**, 6223–6228.

6 Y. Li, X. Zhang, T. Zou, Q. Mu and J. Yang, *ACS Appl. Mater. Interfaces*, 2022, **14**, 21758–21767.

7 H. Liu, Z. Sun, Y. Chen, W. Zhang, X. Chen and C.-P. Wong, *ACS Nano*, 2022, **16**, 10088–10129.

8 A. Vailionis, E. G. Gamaly, V. Mizeikis, W. Yang, A. V. Rode and S. Juodkazis, *Nat. Commun.*, 2011, **2**, 445.

9 H. B. Sun, Y. Xu, S. Juodkazis, K. Sun, M. Watanabe, S. Matsuo, H. Misawa and J. Nishii, *Opt. Lett.*, 2001, **26**, 325–327.

10 Z. Z. Li, L. Wang, H. Fan, Y. H. Yu, H. B. Sun, S. Juodkazis and Q. D. Chen, *Light: Sci. Appl.*, 2020, **9**, 41.

11 K. Sugioka, *Int. J. Extreme Manuf.*, 2019, **1**, 012003.

12 F. Sima, K. Sugioka, R. M. Vazquez, R. Osellame, L. Kelemen and P. Ormos, *Nanophotonics*, 2018, **7**, 613–634.

13 M. Malinauskas, A. Zukauskas, S. Hasegawa, Y. Hayasaki, V. Mizeikis, R. Buividas and S. Juodkazis, *Light: Sci. Appl.*, 2016, **5**, e16133.

14 J. B. Yu, M. T. Luo, Z. Y. Lv, S. M. Huang, H. H. Hsu, C. C. Kuo, S. T. Han and Y. Zhou, *Nanoscale*, 2020, **12**, 23391–23423.

15 M. Xi, J. L. Yong, F. Chen, Q. Yang and X. Hou, *RSC Adv.*, 2019, **9**, 6650–6657.

16 G. Wen, Z. G. Guo and W. M. Liu, *Nanoscale*, 2017, **9**, 3338–3366.

17 Z. W. Mao, W. Cao, J. Hu, L. Jiang, A. D. Wang, X. Li, J. Cao and Y. F. Lu, *RSC Adv.*, 2017, **7**, 49649–49654.

18 Y. Lu, L. D. Yu, Z. Zhang, S. Z. Wu, G. Q. Li, P. C. Wu, Y. L. Hu, J. W. Li, J. R. Chu and D. Wu, *RSC Adv.*, 2017, **7**, 11170–11179.

19 M. S. S. Bharati, B. Chandu and S. V. Rao, *RSC Adv.*, 2019, **9**, 1517–1525.

20 M. F. El-Kady, M. Ihns, M. Li, J. Y. Hwang, M. F. Mousavi, L. Chaney, A. T. Lech and R. B. Kaner, *Proc. Natl. Acad. Sci. U. S. A.*, 2015, **112**, 4233–4238.

21 J. Xu, X. L. Li, Y. Zhong, J. Qi, Z. H. Wang, Z. F. Chai, W. W. Li, C. B. Jing and Y. Cheng, *Adv. Mater. Technol.*, 2018, **3**, 1800372.

22 H. Ceylan, N. O. Dogan, I. C. Yasa, M. N. Musaoglu, Z. U. Kulali and M. Sitti, *Sci. Adv.*, 2021, **7**, eabh0273.

23 Y. Wei, Q. Yang, H. Bian, F. Chen, M. Li, Y. Dai and X. Hou, *Appl. Surf. Sci.*, 2018, **457**, 1202–1207.

24 C. Wang, L. Yang, Y. Hu, S. Rao, Y. Wang, D. Pan, S. Ji, C. Zhang, Y. Su, W. Zhu, J. Li, D. Wu and J. Chu, *ACS Nano*, 2019, **13**, 4667–4676.

25 F. Jin, J. Liu, Y.-Y. Zhao, X.-Z. Dong, M.-L. Zheng and X.-M. Duan, *Nat. Commun.*, 2022, **13**, 1357.

26 Y. Z. Liu, *Int. J. Mach. Tools Manuf.*, 2020, **150**, 103510.

27 X. Q. Liu, B. F. Bai, Q. D. Chen and H. B. Sun, *Opto-Electron. Adv.*, 2019, **2**, 190021.

28 M. Chambonneau, D. Grojo, O. Tokel, F. O. Ilday, S. Tzortzakis and S. Nolte, *Laser Photonics Rev.*, 2021, **15**, 2100140.

29 X. W. Li, Q. Xie, L. Jiang, W. N. Han, Q. S. Wang, A. D. Wang, J. Hu and Y. F. Lu, *Appl. Phys. Lett.*, 2017, **110**, 181907.

30 Z. J. Lin, J. Xu, Y. P. Song, X. L. Li, P. Wang, W. Chu, Z. H. Wang and Y. Cheng, *Adv. Mater. Technol.*, 2020, **5**, 1900989.

31 A. Marcinkevicius, S. Juodkazis, M. Watanabe, M. Miwa, S. Matsuo, H. Misawa and J. Nishii, *Opt. Lett.*, 2001, **26**, 277–279.

32 X.-W. Cao, Q.-D. Chen, H. Fan, L. Zhang, S. Juodkazis and H.-B. Sun, *Nanomaterials*, 2018, **8**, 287.

33 X. Q. Liu, L. Yu, Q. D. Chen and H. B. Sun, *Appl. Phys. Lett.*, 2017, **110**, 091602.

34 X. Q. Liu, Q. D. Chen, K. M. Guan, Z. C. Ma, Y. H. Yu, Q. K. Li, Z. N. Tian and H. B. Sun, *Laser Photonics Rev.*, 2017, **11**, 1600115.

35 J. H. Noh, J. D. Fowlkes, R. Timilsina, M. G. Stanford, B. B. Lewis and P. D. Rack, *ACS Appl. Mater. Interfaces*, 2015, **7**, 4179–4184.

36 H. G. Liu, Y. Li, W. X. Lin and M. H. Hong, *Opt. Laser Technol.*, 2020, **132**, 106472.

37 L. Chen and D. Q. Yu, *J. Mater. Sci.: Mater. Electron.*, 2021, **32**, 16481–16493.

38 X. L. Li, J. Xu, Z. J. Lin, J. Qi, P. Wang, W. Chu, Z. W. Fang, Z. H. Wang, Z. F. Chai and Y. Cheng, *Appl. Surf. Sci.*, 2019, **485**, 188–193.

39 K. Kurihara, T. Nakano, H. Ikeya, M. Ujiie and J. Tominaga, *Microelectron. Eng.*, 2008, **85**, 1197–1201.

40 A. Nishiguchi, A. Mourran, H. Zhang and M. Moller, *Adv. Sci.*, 2018, **5**, 1700038.

41 R. Batchelor, T. Messer, M. Hippler, M. Wegener, C. Barner-Kowollik and E. Blasco, *Adv. Mater.*, 2019, **31**, 1904085.

42 V. F. Paz, M. Emons, K. Obata, A. Ovsianikov, S. Peterhansel, K. Frenner, C. Reinhardt, B. Chichkov, U. Morgner and W. Osten, *J. Laser Appl.*, 2012, **24**, 042004.

43 R. Infuehr, N. Pucher, C. Heller, H. Lichtenegger, R. Liska, V. Schmidt, L. Kuna, A. Haase and J. Stampfl, *Appl. Surf. Sci.*, 2007, **254**, 836–840.

44 K. Obata, A. El-Tamer, L. Koch, U. Hinze and B. N. Chichkov, *Light: Sci. Appl.*, 2013, **2**, e116.

45 S. K. Saha, D. Wang, V. H. Nguyen, Y. Chang, J. S. Oakdale and S.-C. Chen, *Science*, 2019, **366**, 105–109.

46 G. L. Roth, C. Esen and R. Hellmann, *Opt. Express*, 2017, **25**, 18442–18450.

47 O. I. Avila, N. B. Tomazio, A. J. G. Otuka, J. C. Stefanelo, M. B. Andrade, D. T. Balogh and C. R. Mendonca, *J. Polym. Sci., Part B: Polym. Phys.*, 2018, **56**, 479–483.

48 A. Zhizhchenko, A. Kuchmizhak, O. Vitrik, Y. Kulchin and S. Juodkazis, *Nanoscale*, 2018, **10**, 21414–21424.

49 J. H. Li, C. T. Wu, P. K. Chu and M. Gelinsky, *Mater. Sci. Eng., R*, 2020, **140**, 100543.

50 J. F. Xing, M. L. Zheng and X. M. Duan, *Chem. Soc. Rev.*, 2015, **44**, 5031–5039.

51 M. Umar, K. Min and S. Kim, *APL Photonics*, 2019, **4**, 120901.

52 P. Kunwar, Z. Xiong, Y. Zhu, H. Y. Li, A. Filip and P. Soman, *Adv. Opt. Mater.*, 2019, **7**, 1900656.

53 J. P. Aguilar, M. Lipka, G. A. Primo, E. E. Licon-Bernal, J. M. Fernandez-Pradas, A. Yaroshchuk, F. Albericio and A. Mata, *Adv. Funct. Mater.*, 2018, **28**, 1870158.

54 C. Kerse, H. Kalaycioglu, P. Elahi, B. Cetin, D. K. Kesim, O. Akcaalan, S. Yavas, M. D. Asik, B. Oktem, H. Hoogland, R. Holzwarth and F. O. Ilday, *Nature*, 2016, **537**, 84–88.

55 G. Bonamis, K. Mishchick, E. Audouard, C. Honninger, E. Mottay, J. Lopez and I. Manek-Honninger, *J. Laser Appl.*, 2019, **31**, 022205.

56 E. Kifle, P. Loiko, C. Romero, J. R. V. d. Aldana, M. Aguilo, F. Diaz, P. Camy, U. Griebner, V. Petrov and X. Mateos, *Prog. Quantum Electron.*, 2020, **72**, 100266.

57 D. Metzner, P. Lickschat and S. Weissmantel, *J. Laser Appl.*, 2021, **33**, 012057.

58 I. Kuznetsov, I. Mukhin, O. Palashov and K.-I. Ueda, *Opt. Lett.*, 2018, **43**, 3941–3944.

59 M. Kienel, M. Mueller, A. Klenke, J. Limpert and A. Tuennermann, *Opt. Lett.*, 2016, **41**, 3343–3346.

60 L.-J. He, K. Liu, Y. Bo, Z. Liu, X.-J. Wang, F. Yang, L. Yuan, Q.-J. Peng, D.-F. Cui and Z.-Y. Xu, *Opt. Lett.*, 2018, **43**, 539–542.

61 Z. Yin, J. Ma, J. Wang, P. Yuan, G. Xie and L. Qian, *IEEE Photonics J.*, 2019, **11**, 1503612.

62 J. G. Ma, J. Wang, P. Yuan, G. Q. Xie, K. N. Xiong, Y. F. Tu, X. N. Tu, E. W. Shi, Y. Q. Zheng and L. J. Qian, *Optica*, 2015, **2**, 1006–1009.

63 J. G. Ma, J. Wang, P. Yuan, G. Q. Xie and L. J. Qian, *Chin. Opt. Lett.*, 2017, **15**, 021901.

64 J. G. Ma, J. Wang, B. J. Zhou, P. Yuan, G. Q. Xie, K. N. Xiong, Y. Q. Zheng, H. Y. Zhu and L. J. Qian, *Opt. Express*, 2017, **25**, 25149–25164.

65 A. J. Gross and K. Bertoldi, *Small*, 2019, **15**, 1902370.

66 Q. Geng, D. Wang, P. Chen and S.-C. Chen, *Nat. Commun.*, 2019, **10**, 2179.

67 D. Yang, L. Liu, Q. Gong and Y. Li, *Macromol. Rapid Commun.*, 2019, **40**, 1900041.

68 Z.-Y. Hu, H. Ren, H. Xia, Z.-N. Tian, J.-L. Qi, M. Wen, Q.-D. Chen and H.-B. Sun, *J. Lightwave Technol.*, 2021, **39**, 2091–2098.

69 C. Zhu, Y. Li, H. Yuan, Y. Wang, L. Liang, X. Sun and W. Wang, *Optik*, 2021, **242**, 166991.

70 J. Li, Y. Tang, Z. Kuang, J. Schille, U. Loeschner, W. Perrie, D. Liu, G. Dearden and S. Edwardson, *Opt. Lasers Eng.*, 2019, **112**, 59–67.

71 Z. Luo, J. a. Duan and C. Guo, *Opt. Lett.*, 2017, **42**, 2358–2361.

72 Q. Xie, X. Li, L. Jiang, B. Xia, X. Yan, W. Zhao and Y. Lu, *Appl. Phys. A: Mater. Sci. Process.*, 2016, **122**, 136.

73 G.-L. Roth, S. Rung, C. Esen and R. Hellmann, *Opt. Express*, 2020, **28**, 5801–5811.

74 Y. Hu, Y. Chen, J. Ma, J. Li, W. Huang and J. Chu, *Appl. Phys. Lett.*, 2013, **103**, 141112.

75 J. Finger and M. Hesker, *J. Phys.: Photonics*, 2021, **3**, 021004.

76 A. Žemaitis, M. Gaidys, P. Gecys, G. Raciukaitis and M. Gedvilas, *Opt. Lasers Eng.*, 2019, **114**, 83–89.

77 Y. Yao, Y. He, D. Qi, F. Cao, J. Yao, P. Ding, C. Jin, X. Wu, L. Deng, T. Jia, F. Huang, J. Liang, Z. Sun and S. Zhang, *ACS Photonics*, 2021, **8**, 738–744.

78 W. Q. Zhao and Z. S. Yu, *Opt. Lasers Eng.*, 2018, **105**, 125–131.

79 Y. G. Chen, Y. J. Cao, Y. G. Wang, L. G. Zhang, G. Shao and J. F. Zi, *Ceram. Int.*, 2020, **46**, 11747–11761.

80 P. Fan, B. Bai, M. Zhong, H. Zhang, J. Long, J. Han, W. Wang and G. Jin, *ACS Nano*, 2017, **11**, 7401–7408.

81 Y. Hu, H. Yuan, S. Liu, J. Ni, Z. Lao, C. Xin, D. Pan, Y. Zhang, W. Zhu, J. Li, D. Wu and J. Chu, *Adv. Mater.*, 2020, **32**, 2002356.

82 J. Yong, F. Chen, Q. Yang, Y. Fang, J. Huo, J. Zhang and X. Hou, *Adv. Mater. Interfaces*, 2017, **4**, 1700552.

83 A. K. M. R. H. Chowdhury, B. Tan and K. Venkatakrishnan, *ACS Appl. Mater. Interfaces*, 2017, **9**, 19662–19676.

84 P. Dharmalingam, K. Venkatakrishnan and B. Tan, *ACS Nano*, 2021, **15**, 9967–9986.

85 J. L. Yong, Q. Yang, C. L. Guo, F. Chen and X. Hou, *RSC Adv.*, 2019, **9**, 12470–12495.

86 Z. Zhang, Y. H. Zhang, H. Fan, Y. L. Wang, C. Zhou, F. F. Ren, S. Z. Wu, G. Q. Li, Y. L. Hu, J. W. Li, D. Wu and J. R. Chu, *Nanoscale*, 2017, **9**, 15796–15803.

87 Z. Yu, J. Hu and K. M. Li, *J. Mater. Process. Technol.*, 2019, **268**, 10–17.

88 Q. Li, L. J. Yang, C. J. Hou, O. Adeyemi, C. Y. Chen and Y. Wang, *Opt. Lasers Eng.*, 2019, **114**, 22–30.

89 Z. Y. Zhai, W. J. Wang, X. S. Mei, M. Li and X. Li, *Optik*, 2019, **194**, 163066.

90 T. V. Kononenko, C. Freitag, D. N. Sovyk, A. B. Lukhter, K. V. Skvortsov and V. I. Konov, *Opt. Lasers Eng.*, 2018, **103**, 65–70.

91 R. J. Wang, X. Dong, K. D. Wang, X. M. Sun, Z. J. Fan and W. Q. Duan, *Int. J. Adv. Manuf. Technol.*, 2021, **114**, 857–869.

92 R. J. Wang, X. Dong, K. D. Wang, X. M. Sun, Z. J. Fan and W. Q. Duan, *Opt. Lasers Eng.*, 2019, **121**, 406–415.

93 J. Yong, J. Huo, Q. Yang, F. Chen, Y. Fang, X. Wu, L. Liu, X. Lu, J. Zhang and X. Hou, *Adv. Mater. Interfaces*, 2018, **5**, 1701479.

94 H. R. Wang, F. Zhang, K. W. Ding and J. Duan, *Optik*, 2021, **229**, 166295.

95 J. L. Yong, F. Chen, J. L. Huo, Y. Fang, Q. Yang, J. Z. Zhang and X. Hou, *Nanoscale*, 2018, **10**, 3688–3696.

96 N. F. Ren, K. B. Xia, H. Y. Yang, F. Q. Gao and S. W. Song, *Ceram. Int.*, 2021, **47**, 11465–11473.

97 L. S. Jiao, H. Y. Zheng, Y. L. Zhang and E. Y. K. Ng, *SN Appl. Sci.*, 2019, **1**, 80.

98 Y. Fang, J. L. Yong, Y. Cheng, Q. Yang, X. Hou and F. Chen, *Adv. Mater. Interfaces*, 2021, **8**, 2001334.

99 K. Mishchik, K. Gaudfrin and J. Lopez, *J. Laser Micro/Nanoeng.*, 2017, **12**, 321–324.

100 G. Fu, L. L. Ma, F. F. Su and M. Shi, *Optoelectron. Lett.*, 2018, **14**, 212–215.

101 J. F. Lu, Y. Dai, Q. Li, Y. L. Zhang, C. H. Wang, F. F. Pang, T. Y. Wang and X. L. Zeng, *Nanoscale*, 2019, **11**, 908–914.

102 H. Q. Xie, C. K. Zhang, R. Wang, H. Tang, M. D. Mu, H. S. Li, Y. P. Guo, L. Yang and K. L. Tang, *Colloids Surf., B*, 2021, **208**, 112021.

103 P. Chen, M. Miyake, M. Tsukamoto, Y. Tsutsumi and T. Hanawa, *J. Biomed. Mater. Res. A*, 2017, **105**, 3456–3464.

104 Q. Wang and W. Zhou, *Opt. Mater.*, 2017, **72**, 508–512.

105 Q.-K. Li, J.-J. Cao, Y.-H. Yu, L. Wang, Y.-L. Sun, Q.-D. Chen and H.-B. Sun, *Opt. Lett.*, 2017, **42**, 543–546.

106 H. Liu, J. Hu, L. Jiang, S. Zhan, Y. Ma, Z. Xu and Y. Lu, *Appl. Surf. Sci.*, 2020, **528**, 146804.

107 D. Jiang, P. Fan, D. Gong, J. Long, H. Zhang and M. Zhong, *J. Mater. Process. Technol.*, 2016, **236**, 56–63.

108 R. Pan, H. Zhang and M. Zhong, *ACS Appl. Mater. Interfaces*, 2021, **13**, 1743–1753.

109 Y. Xiao, X. Zhang, R. Li, H. Liu, N. Zhou and J. Zhang, *Vacuum*, 2021, **184**, 109987.

110 M. Cui, T. Huang, R. Xiao, X. Zhang, X. Qin, Q. Zhang, J. Xu and Q. Wu, *ACS Sustainable Chem. Eng.*, 2019, **7**, 14669–14676.

111 S. Kwon, G. Kim, H. Lim, J. Kim, K. B. Choi and J. Lee, *Appl. Phys. Lett.*, 2018, **113**, 243901.

112 J. Heitz, C. Plamadeala, M. Wiesbauer, P. Freudenthaler, R. Wollhofen, J. Jacak, T. A. Klar, B. Magnus, D. Koestner, A. Weth, W. Baumgartner and R. Marksteiner, *J. Biomed. Mater. Res. A*, 2017, **105**, 891–899.

113 A. Trautmann, M. Rueth, H.-D. Lemke, T. Walther and R. Hellmann, *Opt. Laser Technol.*, 2018, **106**, 474–480.

114 X. Huang, Y. Zhang, M. Shi, L.-P. Zhang, Y. Zhang and Y. Zhao, *Eur. Polym. J.*, 2021, **153**, 110505.

115 Z. N. Yang, P. F. Ji, Z. Zhang, Y. D. Ju, Z. Wang, Q. Zhang, C. C. Wang and W. Xu, *Opt. Commun.*, 2020, **475**, 126237.

116 K. K. Kumar, G. L. Samuel and M. S. Shunmugam, *J. Mater. Process. Technol.*, 2019, **263**, 266–275.

117 C. Q. Min, X. B. Yang, M. Xue, Q. S. Li, W. J. Wang and X. S. Mei, *Ceram. Int.*, 2021, **47**, 461–469.

118 R. J. Wang, X. Dong, K. D. Wang, X. M. Sun, Z. J. Fan, W. Q. Duan and M. B. G. Jun, *Appl. Surf. Sci.*, 2021, **537**, 148001.

119 Y. X. Duan, G. C. You, K. E. Sun, Z. Zhu, X. Q. Liao, L. F. Lv, H. Tang, B. Xu and L. He, *Nanoscale Adv.*, 2021, **3**, 6271–6293.

120 L. He, H. Liu, W. Luo, W. C. Zhang, X. B. Liao, Y. Q. Guo, T. J. Hong, H. Yuan and L. Mai, *Appl. Phys. Lett.*, 2019, **114**, 223903.

121 Z. Liu, X. Yuan, S. Zhang, J. Wang, Q. Huang, N. Yu, Y. Zhu, L. Fu, F. Wang, Y. Chen and Y. Wu, *NPG Asia Mater.*, 2019, **11**, 12.

122 W. Yang, Y. X. Zhu, Z. F. Jia, L. He, L. Xu, J. S. Meng, M. Tahir, Z. X. Zhou, X. W. Wang and L. Q. Mai, *Adv. Energy Mater.*, 2020, **10**, 2001873.

123 L. He, T. J. Hong, X. F. Hong, X. B. Liao, Y. M. Chen, W. C. Zhang, H. Liu, W. Luo and L. Q. Mai, *Energy Technol.*, 2019, **7**, 1900144.

124 Z. Zhu, R. Y. Kan, P. J. Wu, Y. Ma, Z. Y. Wang, R. H. Yu, X. B. Liao, J. S. Wu, L. He, S. Hu and L. Q. Mai, *Small*, 2021, **17**, 2103136.

125 Y. Zheng, H. J. Seifert, H. Shi, Y. Zhang, C. Kubel and W. Pfleging, *Electrochim. Acta*, 2019, **317**, 502–508.

126 N. Kurra, Q. Jiang, P. Nayak and H. N. Alshareef, *Nano Today*, 2019, **24**, 81–102.

127 Y. Wang, X. F. Hong, Y. Q. Guo, Y. L. Zhao, X. B. Liao, X. Liu, Q. Li, L. He and L. Q. Mai, *Small*, 2020, **16**, 2000293.

128 U. Staudinger, G. Zyla, B. Krause, A. Janke, D. Fischer, C. Esen, B. Voit and A. Ostendorf, *Microelectron. Eng.*, 2017, **179**, 48–55.

129 S. T. Wang, Y. C. Yu, R. Z. Li, G. Y. Feng, Z. L. Wu, G. Compagnini, A. Gulino, Z. L. Feng and A. M. Hu, *Electrochim. Acta*, 2017, **241**, 153–161.

130 B. Dorin, P. Parkinson and P. Scully, *J. Mater. Chem. C*, 2017, **5**, 4923–4930.

131 S. Kim, J. Kim, Y. H. Joung, S. Ahn, C. Park, J. Choi and C. Koo, *Lab Chip*, 2020, **20**, 4474–4485.

132 F. Chen, C. Shan, K. Liu, Q. Yang, X. Meng, S. He, J. Si, F. Yun and X. Hou, *Opt. Lett.*, 2013, **38**, 2911–2914.

133 C. Z. Liao, A. Wuethrich and M. Trau, *Appl. Mater. Today*, 2020, **19**, 100635.

134 C. W. Wang, L. Yang, C. C. Zhang, S. L. Rao, Y. L. Wang, S. Z. Wu, J. W. Li, Y. L. Hu, D. Wu, J. R. Chu and K. Sugioka, *Microsyst. Nanoeng.*, 2019, **5**, 17.

135 H. Wang, Y. L. Zhang, W. Wang, H. Ding and H. B. Sun, *Laser Photonics Rev.*, 2017, **11**, 1600116.

136 A. Sontheimer-Phelps, B. A. Hassell and D. E. Ingber, *Nat. Rev. Cancer*, 2019, **19**, 65–81.

137 F. Sima, H. Kawano, A. Miyawaki, L. Kelemen, P. Ormos, D. Wu, J. Xu, K. Midorikawa and K. Sugioka, *ACS Appl. Bio Mater.*, 2018, **1**, 1667–1676.

138 Z. X. Lao, Y. Y. Zheng, Y. C. Dai, Y. L. Hu, J. C. Ni, S. Y. Ji, Z. Cai, Z. J. Smith, J. W. Li, L. Zhang, D. Wu and J. R. Chu, *Adv. Funct. Mater.*, 2020, **30**, 1909467.

139 O. Kopach, K. Zheng, O. A. Sindeeva, M. Gai, G. B. Sukhorukov and D. A. Rusakov, *Biomater. Sci.*, 2019, **7**, 2358–2371.

140 Y. L. Hu, S. L. Rao, S. Z. Wu, P. F. Wei, W. X. Qiu, D. Wu, B. Xu, J. C. Ni, L. Yang, J. W. Li, J. R. Chu and K. Sugioka, *Adv. Opt. Mater.*, 2018, **6**, 1701299.

141 F. Zhang, C. Wang, K. Yin, X. R. Dong, Y. X. Song, Y. X. Tian and J. A. Duan, *Sci. Rep.*, 2018, **8**, 2419.

142 M. Li, Q. Yang, F. Chen, J. Yong, H. Bian, Y. Wei, Y. Fang and X. Hou, *Adv. Eng. Mater.*, 2019, **21**, 1800994.

143 J.-J. Cao, Z.-S. Hou, Z.-N. Tian, J.-G. Hua, Y.-L. Zhang and Q.-D. Chen, *ACS Appl. Mater. Interfaces*, 2020, **12**, 10107–10117.

144 X.-Q. Liu, L. Yu, S.-N. Yang, Q.-D. Chen, L. Wang, S. Juodkazis and H.-B. Sun, *Laser Photonics Rev.*, 2019, **13**, 1800272.

145 C. M. B. Ho, A. Mishra, K. Hu, J. An, Y.-J. Kim and Y.-J. Yoon, *ACS Biomater. Sci. Eng.*, 2017, **3**, 2198–2214.

146 J. R. Thompson, K. S. Worthington, B. J. Green, N. K. Mullin, C. Jiao, E. E. Kaalberg, L. A. Wiley, I. C. Han, S. R. Russell, E. H. Sohn, C. A. Guymon, R. F. Mullins, E. M. Stone and B. A. Tucker, *Acta Biomater.*, 2019, **94**, 204–218.

147 B. Richter, V. Hahn, S. Bertels, T. K. Claus, M. Wegener, G. Delaittre, C. Barner-Kowollik and M. Bastmeyer, *Adv. Mater.*, 2017, **29**, 1604342.

148 J. Song, C. Michas, C. S. Chen, A. E. White and M. W. Grinstaff, *Adv. Healthcare Mater.*, 2020, **9**, 1901217.

149 A. Daskalova, B. Ostrowska, A. Zhelyazkova, W. Swieszkowski, A. Trifonov, H. Declercq, C. Nathala, K. Szlazak, M. Lojkowski, W. Husinsky and I. Buchvarov, *Appl. Phys. A: Mater. Sci. Process.*, 2018, **124**, 413.

150 S. Jeon, S. Kim, S. Ha, S. Lee, E. Kim, S. Y. Kim, S. H. Park, J. H. Jeon, S. W. Kim, C. Moon, B. J. Nelson, J. Y. Kim, S. W. Yu and H. Choi, *Sci. Robot.*, 2019, **4**, eaav4317.

151 Y. L. Zhang, Y. Tian, H. Wang, Z. C. Ma, D. D. Han, L. G. Niu, Q. D. Chen and H. B. Sun, *ACS Nano*, 2019, **13**, 4041–4048.

152 Z. C. Ma, Y. L. Zhang, B. Han, X. Y. Hu, C. H. Li, Q. D. Chen and H. B. Sun, *Nat. Commun.*, 2020, **11**, 4536.

153 J. Yu, L. Jiang, J. Yan and W. Li, *ACS Biomater. Sci. Eng.*, 2020, **6**, 6445–6452.

154 C. De Marco, S. M. Eaton, R. Suriano, S. Turri, M. Levi, R. Ramponi, G. Cerullo and R. Osellame, *ACS Appl. Mater. Interfaces*, 2010, **2**, 2377–2384.